Structural information of composites from complex-valued measured bulk properties

Christian Engström

Electromagnetic Theory
Department of Electrical and Information Technology
Lund University
Sweden
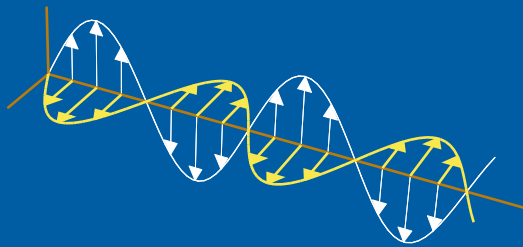
Christian Engström
christian.engstrom@es.lth.se

Department of Electrical and Information Technology
Electromagnetic Theory
Lund University
P.O. Box 118
SE-221 00 Lund
Sweden

Abstract

This paper is concerned with the estimation of the volume fraction and the anisotropy of a two-component composite from measured bulk properties. An algorithm that takes into account that measurements have errors is developed. This algorithm is used to study data from experimental measurements with an unknown microstructure. The dependence on the microstructure is quantified in terms of a measure in the representation formula introduced by D. Bergman. We use composites with known microstructures to illustrate the dependence on the underlying measure and show how errors in the measurements affect the estimations of the structural parameters.

1   Introduction

In two previous papers [7, 8], we discussed the possibility of bounding structural parameters, such as the volume fraction and the anisotropy of a two-component composite, from measurements of bulk properties. In practice, we have to take into account that measurements have errors.

The geometry of the microstructure can be described by a particular positive measure on the interval $[0, 1]$. The determination of this measure from measurements of bulk properties is by some authors called inverse homogenization. Various inverse algorithms for recovering the measure of composites from experimental data have been developed [3, 5, 6]. When the measure is recovered the volume fraction and the anisotropy of the material are given by the first two moments of the measure.

Instead of seeking the measure, the measured bulk properties can be used to bound the structural parameters. In other words, restrictions on the moments of the measure are derived directly. The advantage with this approach is that it can be used even if we have limited information from measurements (few or inaccurate measurements). Inverse bounds for the volume fraction were first derived in [12, 13]. The authors use Milton's and Bergman's bounds in an inverse way to bound the volume fraction from experimental data. Explicit formulas for bounds on the volume fraction can in the case of measurements of lossy materials be found in reference [4, 8]. These inverse bounds cannot be used directly, when there are uncertainties in the measurements.

Here we develop a numerical method based on the inverse bounds in reference [8] to derive bounds, not only on the structural parameters but also on the values of the components in the composite. These bounds are derived from measurements of the complex permittivity at different frequencies or at different volume fractions. Error estimates are assumed to be available for the components and for the effective permittivity of the composite. We use measured bulk properties from two experiments. One experiment was in the optical region and in the second experiment a microwave source was used.

In many cases partial information about the microstructure is available. For example, in the random case, the composite is usually known to be approximately isotropic. This knowledge can be used to derive tighter bounds on the volume frac-

tion. If the volume fraction is approximately known, the bounds on the anisotropy parameter become tighter.

Before proceeding to this problem, we discuss properties of the underlying measure (the spectral density function) that characterize the microstructure. Moreover, we show that the tightness of the bounds on the structural parameters is sensitive to the microstructure. Numerical experiments with known microstructures are used to illustrate this dependence on the spectral density function and show how errors in the measurements affect the tightness of the bounds.

2   Representation of the effective permittivity

The materials in this paper are assumed to be d-dimensional and to consist of two homogeneous and isotropic phases. The two-component material is locally modeled by the scalar relative permittivity

$$\epsilon(\epsilon_1, \epsilon_2) = \epsilon_1 \chi_1(\boldsymbol{x}) + \epsilon_2 \chi_2(\boldsymbol{x}), \tag{2.1}$$

where the components are isotropic with constant permittivity ϵ_1 and ϵ_2. We use complex valued permittivities and assume that the imaginary parts are greater or equal to zero. The volume fraction of phase ϵ_i is denoted f_i and the total volume $f_1 + f_2$ is assumed to be one. Write the complex permittivity of a material on the form

$$\epsilon(\omega) = \epsilon^{\mathrm{r}}(\omega) + \epsilon^{\mathrm{i}}(\omega)\mathrm{i}, \tag{2.2}$$

where $\epsilon^{\mathrm{r}}(\omega)$ and $\epsilon^{\mathrm{i}}(\omega)$ are the real and imaginary parts, respectively, and ω is the angular frequency of the applied field.

We define an effective permittivity ϵ_{e} when the wavelength of the applied field is much longer than the characteristic length of the microstructure. The Herglotz property state that $\mathrm{Im}\{\epsilon_{\mathrm{e}}\} > 0$ when $\mathrm{Im}\{\epsilon_1\} > 0$ and $\mathrm{Im}\{\epsilon_2\} > 0$ [2], that is, the composite dissipates energy when both components dissipate energy. Moreover, the effective permittivity has the homogeneity property $\epsilon_{\mathrm{e}}(c\epsilon_1, c\epsilon_2) = c\epsilon_{\mathrm{e}}(\epsilon_1, \epsilon_2)$ for all complex numbers c. The scaled effective permittivity

$$\frac{\epsilon_{\mathrm{e}}(\epsilon_1, \epsilon_2)}{\epsilon_2} = \epsilon_{\mathrm{e}}\left(\frac{\epsilon_1}{\epsilon_2}, 1\right) \tag{2.3}$$

is analytic in $\epsilon_1/\epsilon_2 \in \mathbb{C}\backslash] - \infty, 0]$ [2, 10]. From the homogeneity property and the Herglotz property Bergman [2] derived a representation of the effective permittivity. In general, the effective permittivity ϵ_{e} has the integral representation [10]

$$\epsilon_{\mathrm{e}}(\epsilon_1, \epsilon_2) = \epsilon_2 - \epsilon_2 G(s), \tag{2.4}$$

where

$$G(s) = \int_0^1 \frac{\mathrm{d}m(y)}{s - y}, \quad s = \frac{\epsilon_2}{\epsilon_2 - \epsilon_1}. \tag{2.5}$$

The positive (Borel) measure m in the integral representation contains all micro structural information. Let s^{r} and s^{i} denote the real and the imaginary parts of the parameter s, and separate the real and imaginary parts of the integrand

$$G(s) = \int_0^1 g_s^{\mathrm{r}}(y)\, \mathrm{d}m(y) - \mathrm{i} \int_0^1 g_s^{\mathrm{i}}(y)\, \mathrm{d}m(y), \tag{2.6}$$

where

$$g_s^{\mathrm{r}}(y) = \frac{s^{\mathrm{r}} - y}{(s^{\mathrm{r}} - y)^2 + (s^{\mathrm{i}})^2}, \quad g_s^{\mathrm{i}}(y) = \frac{s^{\mathrm{i}}}{(s^{\mathrm{r}} - y)^2 + (s^{\mathrm{i}})^2}. \tag{2.7}$$

When $s^{\mathrm{i}} \ll 1$, the function $g_s^{\mathrm{i}}(y)$ approximate the Dirac function $\pi\delta(y - s^{\mathrm{r}})$, in the sense that for any test function $\varphi \in \mathcal{D}(\mathbb{R})$, $(g_s^{\mathrm{i}}, \varphi) \to \pi\varphi(s^{\mathrm{r}})$, when $s^{\mathrm{i}} \to 0$.

Let E denote a measurable set in $[0, 1]$ and fix $y_n \in [0, 1]$. The unit mass concentrated at y_n is defined as $m_{y_n}(E) = 1$ if $y_n \in E$ and $m_{y_n}(E) = 0$ if $y_n \notin E$. Let m be on the form

$$m(E) = \int_E f(y)\, \mathrm{d}\mu(y) + \sum_n \beta_n m_{y_n}(E) \tag{2.8}$$

where μ denotes the Lebesque measure and f is non-negative and integrable over $[0, 1]$. For any test function φ, we have

$$-\frac{1}{\pi} \lim_{\delta \to 0^+} \int_{-\infty}^\infty \operatorname{Im} G(x + \mathrm{i}\delta)\varphi(x)\, \mathrm{d}\mu(x) = \int_0^1 f(x)\varphi(x)\, \mathrm{d}\mu(x) + \sum_n \beta_n \varphi(y_n). \tag{2.9}$$

For example, the effective permittivity for a laminate material is, for fields paralell to the interfaces, the arithmetic mean $\epsilon_{\mathrm{e}} = \epsilon_2 - f_1\epsilon_2/s$. The integral (2.5) then becomes $G(s) = f_1/s$ which gives

$$-\frac{1}{\pi} \int_{-\infty}^\infty \operatorname{Im} G(x + \mathrm{i}\delta)\varphi(x)\, \mathrm{d}\mu(x) = \int_{-\infty}^\infty f_1 \frac{1}{\pi} \frac{\delta}{x^2 + \delta^2} \varphi(x)\, \mathrm{d}\mu(x) \to f_1\varphi(0), \quad \delta \to 0^+. \tag{2.10}$$

We identify a mass f_1 concentrated at $y = 0$, which we denote $m(E) = f_1 m_0(E)$.

When the spectral density function f is continuous and no point masses are present, the formula (2.9) is reduced to Stieltjes inversion formula [1]

$$f(x) = -\frac{1}{\pi} \lim_{\delta \to 0^+} \operatorname{Im} G(x + \delta\mathrm{i}), \quad x \in [0, 1]. \tag{2.11}$$

For example, the two-dimensional checkerboard structure has the exact effective permittivity [15, p. 49]

$$\epsilon_{\mathrm{e}} = \sqrt{\epsilon_1\epsilon_2}. \tag{2.12}$$

From Stieltjes inversion formula follows that the spectral density function f for the checkerboard is

$$f(y) = \frac{1}{\pi}\sqrt{(1 - y)/y}. \tag{2.13}$$

Accurate calculations of the spectral density function f can be obtained if accurate measurements of ϵ_{e} are available for $0 \le s^{\mathrm{r}} \le 1$ and $s^{\mathrm{i}} \ll 1$. In many cases these

measurements are not available and can even be impossible to perform, depending on the dispersion curves for the materials in the composite.

Assume real-valued materials with $\epsilon_2 \geq \epsilon_1$. From the relation $\epsilon_1 \leq \epsilon_e \leq \epsilon_2$ follows

$$0 \leq G(s) \leq \frac{1}{s} \leq 1. \tag{2.14}$$

Let $s = 1 + \delta$, $\delta > 0$. From the inequality above we have

$$1 \geq G(1 + \delta) = \int_0^1 \frac{1}{1 - y + \delta} \, \mathrm{d}m(y) \geq \frac{m\{1\}}{\delta}, \tag{2.15}$$

which implies that the measure m does not have a point mass in $y = 1$, since $\delta > 0$ is arbitrary. The moments of the measure

$$c_{n+1} = (-1)^n \int_0^1 y^n \, \mathrm{d}m(y), \tag{2.16}$$

then vanish in the limit $n \to \infty$. The absolute value of the moments $c_1, c_2, \ldots$ form a non-increasing sequence $|c_1| \geq |c_2| \ldots$. The convergence rate of the moments c_n to zero depend strongly on the support of the measure. If m has no support close to $y = 1$, the convergence is exponential.

Let $s = -1/z$ in the representation (2.5). The integral representation of G is then transformed to

$$\hat{G}(z) = -\frac{1}{z} G(-\frac{1}{z}) = \int_0^1 \frac{\mathrm{d}m(y)}{1 + zy}, \tag{2.17}$$

which is the standard form of a Stieltjes integral representation [1, p. 229].

3 Bounds on the effective permittivity

If partial information, such as the volume fraction, is available about the microstructure, this knowledge can be used to derive bounds on the effective permittivity [2, 14, 15]. We use the Stieltjes series expansion

$$\epsilon_e = \epsilon_2 + \epsilon_2 z \hat{G}(z) = \epsilon_2 F(z), \qquad F(z) = \sum_{n=0}^{\infty} c_n z^n, \tag{3.1}$$

where $z = -1/s = (\epsilon_1 - \epsilon_2)/\epsilon_2$ is the contrast and the coefficients c_n are given by the moments of the measure (2.16). The function $z\hat{G}(z)$ is zero when $z = 0$, implying $c_0 = 1$. The constants c_n depends on the microstructure but not on the values of the two phases. If the microstructure is the same, the single series (3.1) gives the effective permittivity, independent of the value of the phases. The zero-order moment c_1 is the volume fraction f_1 of the phase ϵ_1 and c_2 depends on the anisotropy in the material. In the case of a d-dimensional statistically isotropic composite, the second moment is $-c_1(1 - c_1)/d$ [2, 10].

There are many different methods that gives bounds on the effective properties of the material. In [8] Padé approximations of the Stieltjes series (3.1) were used to derive Milton's and Bergman's well known bounds [2, 14, 15].

The $\epsilon_{p,q}$ Padé approximant to ϵ_e is defined by the equation

$$\epsilon_\mathrm{e}(z)Q(z) - P(z) = \mathcal{O}(z^{p+q+1}) \tag{3.2}$$

where P and Q are polynomials of degree at most p and q, respectively [1]. This equation gives us an approximation of the effective permittivity by the rational function

$$\epsilon_{p,q} = \frac{P(z)}{Q(z)} = \frac{a_0 + ... + a_p z^p}{1 + b_1 z + ... b_q z^q}. \tag{3.3}$$

The sequence of Padé approximations $\epsilon_{M,M}$ and $\epsilon_{M+1,M}$ of the series (3.1) converge, when $M \to \infty$, uniformly to $\epsilon_\mathrm{e}/\epsilon_2$ in any closed finite region of the complex plane cut along the negative real axis from -1 to $-\infty$ [1].

In practice, the volume fraction c_1 is in some cases measured and the composite is in the random case usually assumed to be isotropic. This gives us at most two coefficients in the series expansion, but the rest of the coefficients c_n are in most cases unknown.

The convergence rate of the Padé approximations depends strongly on the value on the contrast z and on the measure m. For $|zy| < 1$ the function $(1 + zy)^{-1}$ has a power expansion in zy. The integral $\hat{G}$ then has the power expansion

$$\hat{G}(z) = \sum_{n=0}^{\infty} (-z)^n \int_0^1 y^n \,\mathrm{d}m(y) = \sum_{n=0}^{\infty} c_{n+1} z^n, \tag{3.4}$$

where (2.16) is used in the last step. The Stieltjes series (3.1) defining the effective permittivity is then convergent. The condition $|zy| < 1$ is satisfied when $|z| < 1$ but also for $0 \le y < \frac{1}{|z|} = |s|$. That is, the series in the representation (3.4) converges if the support of the measure m is in $[0, |s|]$.

In [8] the author derived inverse bounds on the volume fraction and showed that the distance between the bounds rapidly tends to zero for a low contrast material. If very accurate measurements are available for a low contrast material, they give us accurate estimations of the structural parameters, but if the errors in the measurements are not negligible we can get almost anything. Measurements at a low contrast material contain very little information.

The conclusion is, that in most cases data that gives rapid convergence for all measures are not available. The convergence of the series (3.1) and the Padé approximations then depends strongly on the support and the total mass c_1 of the measure. The bounds on the structural parameters c_n are obtained by inverting the bounds on the effective permittivity. The tightness of the bounds on the structural parameters is then dependent on the measure that characterizes the microstructure.

4   Bounds using complex valued measurements

In reference [8] a method to derive bounds on any of the structural parameters c_n is presented. Here we use the bounds on the volume fraction c_1 and on the anisotropy parameter c_2.

Composite	ϵ_1^r	ϵ_1^i	ϵ_2^r	ϵ_2^i
A	3.00	0	2.42	2.89
B	-38.4	2.79	2.98	0

Table 1: Complex permittivity for the two components in two different composites. Composite A is a mix of two dielectrics and composite B is a mix of a metal and a dielectric.

The $\epsilon_{1,1}$ Padé approximant to the series (3.1) gives an upper bound that in the isotropic case corresponds to the upper Hashin-Shtrikman bound [15, p. 574]. The $\epsilon_{1,1}$ Padé approximant can be inverted giving a bound on c_1, [8]. Explicitly, the volume fraction is bounded from below by [4, 8]

$$c_1^{\mathrm{L}} = z^{\mathrm{i}} \frac{(\epsilon_{\mathrm{e}}^{\mathrm{i}} - \epsilon_2^{\mathrm{i}})^2 + (\epsilon_{\mathrm{e}}^{\mathrm{r}} - \epsilon_2^{\mathrm{r}})^2}{|z|^2(\epsilon_{\mathrm{e}}^{\mathrm{i}}\epsilon_2^{\mathrm{r}} - \epsilon_{\mathrm{e}}^{\mathrm{r}}\epsilon_2^{\mathrm{i}})}. \tag{4.1}$$

In the same way, the generalization of the lower Hashin-Shtrikman bound [15, p. 574] can be inverted. Explicitly, the volume fraction is bounded from above by [4, 8]

$$c_1^{\mathrm{U}} = 1 - z^{\mathrm{i}} \frac{(\epsilon_{\mathrm{e}}^{\mathrm{i}} - \epsilon_1^{\mathrm{i}})^2 + (\epsilon_{\mathrm{e}}^{\mathrm{r}} - \epsilon_1^{\mathrm{r}})^2}{|z|^2(\epsilon_{\mathrm{e}}^{\mathrm{r}}\epsilon_1^{\mathrm{i}} - \epsilon_{\mathrm{e}}^{\mathrm{i}}\epsilon_1^{\mathrm{r}})}. \tag{4.2}$$

If the volume fraction c_1 is known we derive bounds on the anisotropy parameter c_2. The $\epsilon_{2,1}$ Padé approximant to the series (3.1) gives an upper bound that in the isotropic case corresponds to the upper Beran bound [15, p. 574]. The $\epsilon_{2,1}$ Padé approximant can be inverted giving a bound on c_2, [8]. Explicit formulas for $c_2^{\mathrm{L}}(c_1)$ and $c_2^{\mathrm{U}}(c_1)$ is presented in the Appendix.

The formulas (4.1) and (4.2) give bounds on the volume fraction c_1, but it is also possible to use $c_2^{\mathrm{L}}(c_1)$ and $c_2^{\mathrm{U}}(c_1)$ to bound the volume fraction in the following way. Let $c_1 \in (0, 1)$ and calculate $c_2^{\mathrm{L}}(\epsilon_1, \epsilon_2, \epsilon_{\mathrm{e}})$ and $c_2^{\mathrm{U}}(\epsilon_1, \epsilon_2, \epsilon_{\mathrm{e}})$ for a fix volume fraction c_1. The bounds on c_2 are required to satisfy the general constraint $-c_1(1 - c_1) \leq c_2 \leq 0$ [2], which restricts the possible values on the volume fraction c_1.

Example As a first illustration, we use the data of composite A in Table 1 and the checkerboard structure (2.12). The effective permittivity is in this case $\epsilon_{\mathrm{e}} = 3.05 + 1.42\mathrm{i}$. The formulas (4.1) and (4.2) imply that the volume fraction is bounded by $0.474 \leq c_1 \leq 0.526$. Using the method above, the bounds $c_2^{\mathrm{L}}(c_1)$ and $c_2^{\mathrm{U}}(c_1)$ provides the same bounds on c_1. Moreover, the anisotropy parameter c_2 is estimated by $-0.139 \leq c_2 \leq -0.110$. The exact values are $c_1 = 0.5$ and $c_2 = -0.125$.

In the case of inaccurate measurements below, the method that uses the bounds on c_2 actually gives the tightest bounds on the volume fraction. Below we use the bounds on c_2 and present calculations using data from measurements.
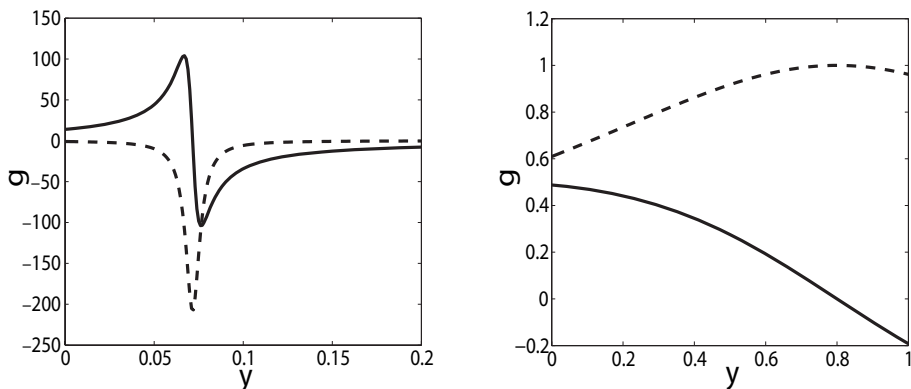
Figure 1: Behavior of the integrand in the integral representation (2.7) for the data presented in Table 1. In both figures, the solid line is the real part and the dashed line is the imaginary part of the integrand. The left graph corresponds to composite B and the right graph corresponds to composite A. The value on the s-parameter for the left graf is $s = 0.072 + 0.005\mathrm{i}$ and the value on s for the right graph is $s = 0.8 - \mathrm{i}$. Note the difference in scale in the two graphs.

5   Structural bounds from measurements

Suppose that error estimates are available for the permittivity of the two components and for the permittivity of the composite. We use uniformly distributed errors and generate independent random numbers for the real and imaginary parts of the measured values. Sweep the volume fraction in the range $0 < c_1 < 1$ and require that the anisotropy parameter c_2 for a fixed value on c_1 satisfy

$$-c_1(1 - c_1) \leq c_2^{\mathrm{L}}(\epsilon_1, \epsilon_2, \epsilon_{\mathrm{e}}) \leq c_2^{\mathrm{U}}(\epsilon_1, \epsilon_2, \epsilon_{\mathrm{e}}) \leq 0, \tag{5.1}$$

where c_2^{L} and c_2^{U}, given in the Appendix, depend on the complex random numbers ϵ_1, ϵ_2 and ϵ_{e}. This requirement gives restrictions on the possible volume fractions c_1 and on the anisotropy parameter c_2. Moreover, we get restrictions on the possible values on the permittivity of the two components and on the effective permittivity of the composite. We present results when the volume fraction is increased from zero to one with a small step, but we have also used random numbers with the same result. Several sets of random numbers of ϵ_1^{r}, ϵ_1^{i}, ϵ_2^{r}, ϵ_2^{i}, $\epsilon_{\mathrm{e}}^{\mathrm{r}}$ and $\epsilon_{\mathrm{e}}^{\mathrm{i}}$ are generated for each fixed number of c_1.

5.1   Numerical examples

The checkerboard structure and a laminate material are used to illustrate the method. We also use an artificial measure to show the dependence of the bounds on the microstructure. We use the values on the two components presented in Table 1 and assume that the errors in all measurements are $\pm 1\%$. The volume fraction is increased from zero to one with the step 10^{-3} or smaller. At each volume fraction c_1, 10^4 random sets of ϵ_1^{r}, ϵ_1^{i}, ϵ_2^{r}, ϵ_2^{i}, $\epsilon_{\mathrm{e}}^{\mathrm{r}}$ and $\epsilon_{\mathrm{e}}^{\mathrm{i}}$ were generated.

5.1.1 The checkerboard

The checkerboard structure (2.12) corresponds exactly to Bruggemans formula [17, p. 463] at the percolation threshold $c_1 = 0.5$. Using the spectral density function for the checkerboard (2.13), the moments of the measure (2.16) are calculated to

$$c_1 = \frac{1}{2}, \quad c_2 = -\frac{1}{8}, \quad c_3 = \frac{1}{16}, \quad \cdots \quad c_{n+1} = \left(\begin{array}{c} 1/2 \\ n+1 \end{array} \right). \tag{5.2}$$

Hence, the moments c_n converge very slowly to zero.

Using the values of the complex permittivity of composite A in Table 1 gives the bounds $0.46 \leq c_1 \leq 0.54$ on the volume fraction and the bounds $-0.15 \leq c_2 \leq -0.10$ on the anisotropy parameter. The arithmetic mean of the frequency distribution of volume fractions is $c_1^{\mathrm{mean}} = 0.5000$. In the previous section we used the same values on ϵ_1, ϵ_2 and ϵ_e, but assumed exact values. The bounds are of course tighter when we have exact values, but we will see below that the value of the contrast $z = (\epsilon_1 - \epsilon_2)/\epsilon_2$ and the measure m also strongly influence the size of the bounds.

The effective permittivity of composite B, in Table 1, is $\epsilon_e = 0.388 + 10.7i$. The values of ϵ_1, ϵ_2 and ϵ_e of composite B imply the bounds $0.018 \leq c_1 \leq 0.99$ on the volume fraction and the bounds $-0.246 \leq c_2 \leq -0.001$ on the anisotropy parameter. The arithmetic mean of the frequency distribution of volume fractions is $c_1^{\mathrm{mean}} = 0.5000$. Notice that the measurements of composite B implies small restrictions on the possible volume fractions and the possible values on the anisotropy parameter c_2. As mentioned above, the exact values are $c_1 = 0.5$ and $c_2 = -0.125$.

The values of the phases in the two composites give very different behavior of the integrands $g_s^{\mathrm{r}}(y)$ and $g_s^{\mathrm{i}}(y)$ in the integral representation (2.7). Figure 1 shows that the integrands test the measure m very differently, which results in different sizes on the bounds on c_1 and on c_2.

The values on the components in composite B gives $s = 0.072 + 0.005i$. In principle, with this small value on the imaginary part of the parameter s the function $g_s^{\mathrm{i}}(y)$ in (2.7) is a good approximation of the Dirac function $\pi\delta(y - 0.072)$. This implies, that the spectral density function f at $y = 0.072$ is approximately

$$f(0.072) \approx -\frac{1}{\pi} \mathrm{Im} \left\{ 1 - \frac{\epsilon_e}{\epsilon_2} \right\}. \tag{5.3}$$

Using exact values on ϵ_1, ϵ_2, and ϵ_e we obtain $f(0.072) \approx 1.143$, which is close to the exact value $f(0.072) = 1.1428$ that is given by (2.13). If the uncertainty in the measurements is 1%, the approximate value on $f(0.072)$ belongs to the intervall $[1.138, 1.148]$. In many cases the uncertainty is much larger, with the uncertainty 5% the value of $f(0.072)$ is estimated to $[1.118, 1.169]$. This shows that in many cases, it is difficult to determine the spectral density function pointwise with high accuracy.

5.1.2 The laminate material

The laminate material has, for the fields parallel to the interfaces, the effective permittivity

$$\epsilon_e = \epsilon_2(1 + c_1 z), \tag{5.4}$$

where we use $c_1 = 0.5$. In this case, only the zero-order moment c_1 is nonzero. The measurements of composite A in Table 1 give the effective permittivity $\epsilon_e = 2.71 + 1.45i$. The bounds on the volume fraction are calculated to $0.490 \leq c_1 \leq 0.507$ and the bounds on the anisotropy parameter are calculated to $-0.01 \leq c_2 \leq 0$. The effective permittivity for composite B, in Table 1, is $\epsilon_e = -17.71 + 1.40i$. From the measurements of composite B we obtain the bounds $0.493 \leq c_1 \leq 0.578$ and $-0.07 \leq c_2 \leq 0$. The exact values are $c_1 = 0.5$ and $c_2 = 0$. Notice that, in this case, the measurements of composite B implies tight bounds on the volume fraction c_1. The bounds on c_2 are much tighter for the laminate material than for the checkerboard structure.

5.1.3 An artificial measure

We choose a spectral density function that has the first and second moment in common with the checkerboard structure. A piecewise constant function with support in $[0, 1/2]$ is

$$f(y) = \begin{cases} 1, & 0 \leq y \leq \frac{1}{2} \\ 0, & \frac{1}{2} < y \leq 1. \end{cases}$$

Using this density function, the moments of the measure (2.16) are calculated to

$$c_1 = \frac{1}{2}, \quad c_2 = -\frac{1}{8}, \quad c_3 = \frac{1}{24}, \quad \cdots \quad c_{n+1} = (-1)^n \frac{\left(\frac{1}{2}\right)^{n+1}}{n+1}. \tag{5.5}$$

Hence, the moments c_n converge exponentially to zero.

Using the spectral function (5.5) and the values of the components in composite A, the effective permittivity (2.4) is calculated to $\epsilon_e = 3.033 + 1.367i$. The bounds on the volume fraction is in this case $0.48 \leq c_1 \leq 0.55$ and the bounds on the anisotropy parameter becomes $-0.138 \leq c_2 \leq -0.095$.

The values of the components in composite B and the spectral function (5.5) give us the effective permittivity $\epsilon_e = 8.274 + 9.108i$. From the measurements of composite B, we obtain the bounds $0.019 \leq c_1 \leq 0.97$ and $-0.248 \leq c_2 \leq -0.001$. The bounds on the structural parameters c_1 and c_2 are close to the bounds using the checkerboard structure. Once again the bounds are not tight when the measurements of composite B are used.

The values of the components in composite B are taken from a real experiment. In the next section we use data from a measurement of the optical properties of a thin film. Composite B in Table 1 corresponds to the measurements at 900 nm in Figure 2.

λ	n_1	k_1	n_2	k_2	n_e	k_e
300	1.53 ± 0.02	1.89 ± 0.01	1.805 ± 0.005	0	1.70 ± 0.01	0.44 ± 0.01
500	1.04 ± 0.02	1.83 ± 0.01	1.745 ± 0.005	0	1.70 ± 0.01	0.52 ± 0.01
700	0.13 ± 0.02	4.10 ± 0.01	1.731 ± 0.005	0	1.62 ± 0.01	0.74 ± 0.01
900	0.18 ± 0.02	5.66 ± 0.03	1.725 ± 0.005	0	1.84 ± 0.01	0.79 ± 0.01

Table 2: Complex refraction index for gold [11], magnesium oxid [16] and for the gold-magnesium oxid composite [9].

5.2 Experimental measurements

We give two examples, where the first is taken from a thin film experiment and in the second experiment a three-dimensional material was measured at microwave frequencies.

5.2.1 Optical source

The optical properties of materials are closely related to their permittivity. The complex index of refraction $N = n + ik$ is

$$N^2 = \epsilon \mu, \tag{5.6}$$

where μ is the magnetic permeability of the material. In the case of non-magnetic materials, $\mu = 1$, we have

$$\epsilon^r = n^2 - k^2, \quad \epsilon^i = 2nk, \tag{5.7}$$

where ϵ^r and ϵ^i are the real and imaginary parts, respectively.

The optical properties of nano-sized gold particles in a magnesium oxide matrix were measured in reference [9]. The gold grains in the composite have a distribution of sizes, with a maximum size of 7 nm. The measured effective refractive index and the refractive index of the two components are presented in Table 2. Using a different approach, the same set of data has previously been studied [12]. In the previous study, no error bars were assigned to the components, but large error bars were assigned to the effective refractive index. We take into account errors in the measurements of the components and assume that the absolute errors in the measurements of the effective refractive index are less than 0.01. The authors in [12] estimated the volume fraction of gold to 0.28. The volume fraction of gold was measured to 0.25, with no error estimates provided [9].

The algorithm described above is used for the data in Table 2. The number of random trials is chosen such that the frequency distribution of c_1 is well described. The volume fraction is increased from zero to one in steps of 10^{-3}. Using typically 5000 random sets, at each volume fraction, the number of points in the frequency distribution is $50\,000 - 130\,000$. It turned out that the measurement at 300 nm gives the tightest bounds on the volume fraction. Figure 3 shows a histogram of the set of estimated volume fractions, where the frequency distribution is described by $134\,000$
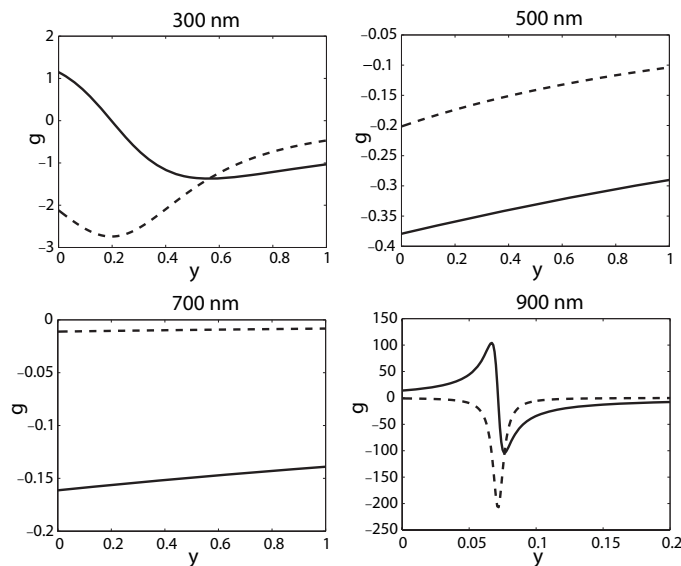
Figure 2: Behavior of the integrand in the integral representation (2.7) for the data presented in Table 2. In all figures, the solid line is the real part and the dashed line is the imaginary part of the integrand. The value on the s-parameter for the four wavelengths 300, 500, 700 and 900 nm are $s = 0.197 + 0.365i$, $s = 0.379 + 0.202i$, $s = 0.161 + 0.011i$, and $s = 0.072 + 0.005i$, respectively. Observe the different scale in the lower right figure.

points. Using the approximate probability density function, the volume fraction is determined to belong to the interval

$$0.18 \leq c_1 \leq 0.32 \tag{5.8}$$

with the probability 95%. Using the measurement at 300 nm the anisotropy parameter is bounded by $-0.091 \leq c_2 \leq -0.022$. The measurement on 500 nm gives the bounds $-0.15 \leq c_2 \leq -0.047$. The intersection of the bounds on c_2 is

$$-0.091 \leq c_2 \leq -0.047. \tag{5.9}$$

The measurements on 700 nm and on 900 nm gives no further restrictions on the structural parameters c_1 and c_2.

The electron micrograph image in [9] shows filaments linking the gold particles, but the composite is most likely isotropic or close to isotropic. The thickness of the film is 150 nm [9]. A relevant question in this context is; is this film two-dimensional? Figure 3 shows $c_2 = -c_1(1 - c_1)/d$ when $d = 2$ and $d = 3$, which corresponds to an isotropic material in two and three dimensions. If we assume that the error in the measured volume fraction $c_1 = 0.25$ is less than 5%, the measurement at 300 nm gives the lower bound $c_2^{\text{low}} = -0.074$. From Figure 3, we conclude the material then should be regarded as three-dimensional.

In reference [12] the authors assume that the material is two-dimensional and isotropic. They estimated the volume fraction to 0.28 but did not established any
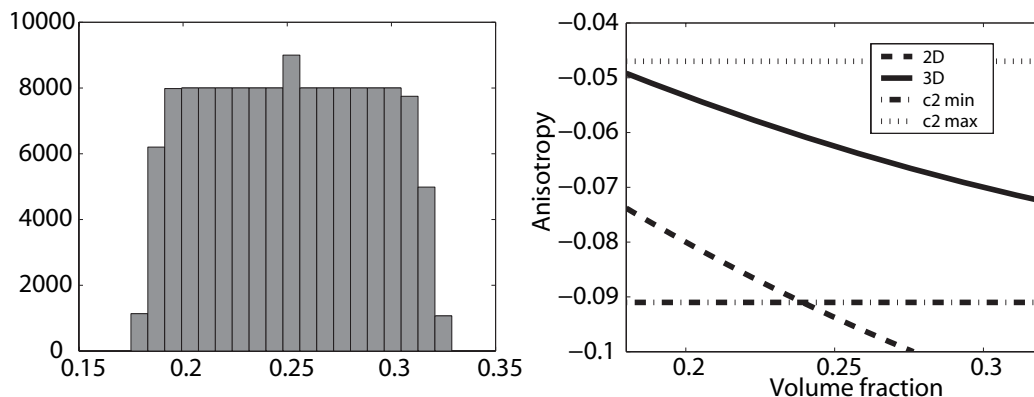
Figure 3: Left: The frequency of volume fractions c_1 lying in the specified intervals for the thin film. Right: The parameter c_2 in the two-dimensional (dashed line) and three-dimensional (solid line) isotropic case. The volume fraction is in the interval (5.8). The lower bound on c_2 (dashed-dotted line) and the upper bound on c_2 (dotted line) are taken from (5.9).

error estimates (only one set of values on the effective refractive index was found within the error bars). A possible explanation for this is that the material should be considered as three-dimensional.

The tightness of the bounds on the structural parameters depends on the uncertainty in the measurements. Above, we assumed that the uncertainty in the measurements of the effective refractive index is less than 0.01. If the uncertainty is larger we obtain less tight estimates of the structural parameters. For example, if the absolute error in all measurements are 0.05 the bounds on the volume fraction become $0.16 \leq c_1 \leq 0.34$.

Tighter bounds on the volume fraction can be obtained from [8] if the material is assumed to be isotropic. A problem with this assumption is that we actually do not know that the material should be regarded as three-dimensional in the full range $300 - 900$ nm. It is possible that the 150 nm thick film behaves as three-dimensional for the shorter wavelengths and as two-dimensional for the longer wavelengths.

5.2.2 Microwave source

In the second example we use data from two composites, where the two samples are composed by the same components, but the volume fractions differ. In each experiment the complex permittivity of an epoxy-aluminium oxide composite was measured at 12 GHz ($\lambda = 2.5\,\text{cm}$). The aluminum oxide is in the form of a fine powder. The particles are in the shape of flakes with a characteristic length not larger than $5\,\mu$m.

We assume that the real parts of ϵ_1, ϵ_2 and ϵ_e were measured with 5% uncertainty. The imaginary parts are usually harder to measure and for that reason we use $\pm 50\%$ times the measured value as the error bars. The measured values on epoxy and on
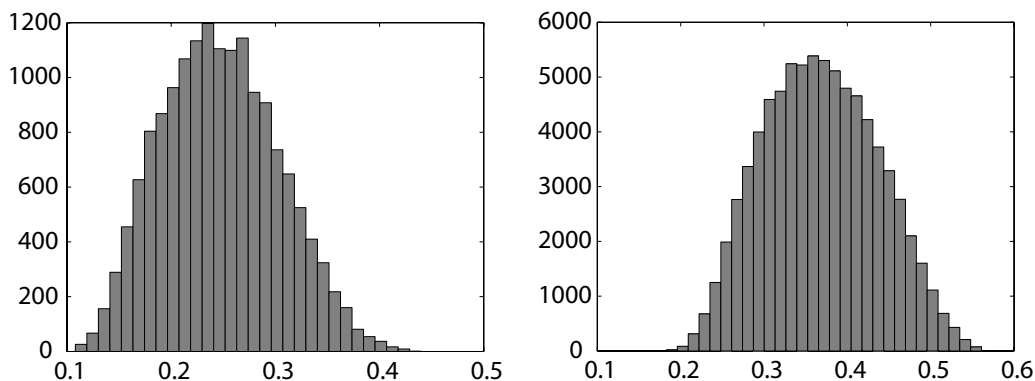
Figure 4: The frequency of volume fractions c_1 lying in the specified intervals. Left: First case, where the volume fraction was measured to $c_1 = 0.20$. Right: Second case, where the volume fraction was measured to $c_1 = 0.30$.

aluminium oxide (Al_2O_3) with the used error estimations are

$$\epsilon_1^{\text{r}} = 9.6 \pm 0.48, \quad \epsilon_1^{\text{i}} = 0.08 \pm 0.04, \quad \epsilon_2^{\text{r}} = 2.814 \pm 0.14, \quad \epsilon_2^{\text{i}} = 0.032 \pm 0.016 \quad (5.10)$$

The effective permittivity of the first sample was measured to $\epsilon_{\text{e}}^{\text{r}} = 3.81 \pm 0.19$ and $\epsilon_{\text{e}}^{\text{i}} = 0.017 \pm 0.0085$. The volume fraction c_1 is increased from zero to one with the step 10^{-3}. Using 10^5 random sets, at each volume fraction, the number of points in the frequency distribution is $16\,000$. The algorithm implies the bounds

$$0.13 \leq c_1 \leq 0.40 \tag{5.11}$$

on the volume fraction and the bounds $-0.21 \leq c_2 \leq -0.007$ on the anisotropy parameter. As before we use 95% probability in the calculations of the bounds. Figure 4 shows the histogram of the frequency of c_1. Moreover, we obtain the restriction $\epsilon_2^{\text{i}} = 0.0194 \pm 0.0034$ on the second phase and the restriction $\epsilon_{\text{e}}^{\text{i}} = 0.0224 \pm 0.0031$ on the effective permittivity. The volume fraction was measured to $c_1 = 0.20$.

The effective permittivity of the second sample was measured to $\epsilon_{\text{e}}^{\text{r}} = 4.383 \pm 0.22$ and $\epsilon_{\text{e}}^{\text{i}} = 0.065 \pm 0.033$. By using the new estimate on ϵ_2^{i} above in the algorithm, we obtain the bounds

$$0.22 \leq c_1 \leq 0.54, \quad -0.23 \leq c_2 \leq -0.007. \tag{5.12}$$

The imaginary part of the effective permittivity is in this case restricted to $\epsilon_{\text{e}}^{\text{i}} = 0.0413 \pm 0.0088$. The volume fraction was measured to $c_1 = 0.30$. Using $2 \cdot 10^4$ random sets, at each volume fraction, the number of points in the frequency distribution is $79\,000$. Figure 4 shows the histogram of the frequency distribution of c_1.

This example shows that the algorithm provides restrictions on the measured values if the error bars are chosen larger than necessary.

6 Discussion and conclusions

We have shown that the inverse bounds derived in [8] can be used to estimate the volume fraction and the anisotropy of two-component composite materials.

The goal with this paper is to show that the inverse bounds can be used even if we have uncertainties in the measurements. The number of random sets was chosen such that the frequency distribution of volume fractions is very well described. This means, we are using far more points than necessary to establish the bounds, but we do not focus on the implementation of an efficient code. The focus is on the connection between the underlying measure and the estimation of the structural parameters. The tightness of the bounds depends on the unknown measure, and measurements at different contrasts of the phases test the measure in different ways. The optimal contrast is probably not available from an experiment. The tightest bounds are obtained if measurements are performed and bounds are calculated at many contrasts, after which the intersection of the bounds is taken. The range of the possible contrasts depends on the dispersion curves of the two materials and the limitation that the homogenization theory is valid.

Moreover, the method also gives restrictions of the possible values on the permittivities. This can be very useful when, for example, the permittivity of one of the components is unknown.

7 Acknowledgements

Appendix

A lower bound $c_2^{\mathrm{L}}(c_1)$ on the anisotropy parameter c_2 is given by

$$c_2^{\mathrm{L}} = -\hat{c}_2 - c_1\hat{c}_1, \quad \text{where} \quad \hat{c}_2 = (T_1 + T_2 + T_3 + T_4)/N \tag{7.1}$$

and

$$
\begin{aligned}
T_1 &= (\epsilon_{\mathrm{e}}^{\mathrm{i}})^2 z^{\mathrm{i}} - 2\epsilon_{\mathrm{e}}^{\mathrm{i}}\epsilon_1^{\mathrm{i}} z^{\mathrm{i}} + (\epsilon_1^{\mathrm{i}})^2 z^{\mathrm{i}} + \hat{c}_1^2(\epsilon_{\mathrm{e}}^{\mathrm{i}})^2(z^{\mathrm{i}})^3 - 2\hat{c}_1\epsilon_1^{\mathrm{i}}(z^{\mathrm{i}})^2\epsilon_{\mathrm{e}}^{\mathrm{r}}, \tag{7.2}\\
T_2 &= z^{\mathrm{i}}(\epsilon_{\mathrm{e}}^{\mathrm{r}})^2 + \hat{c}_1^2(z^{\mathrm{i}})^3(\epsilon_{\mathrm{e}}^{\mathrm{r}})^2 + 2\hat{c}_1\epsilon_{\mathrm{e}}^{\mathrm{i}}(z^{\mathrm{i}})^2\epsilon_1^{\mathrm{r}} - 2z^{\mathrm{i}}\epsilon_{\mathrm{e}}^{\mathrm{r}}\epsilon_1^{\mathrm{r}} + z^{\mathrm{i}}(\epsilon_1^{\mathrm{r}})^2, \tag{7.3}\\
T_3 &= 2\hat{c}_1(\epsilon_{\mathrm{e}}^{\mathrm{i}})^2 z^{\mathrm{i}} z^{\mathrm{r}} - 2\hat{c}_1\epsilon_{\mathrm{e}}^{\mathrm{i}}\epsilon_1^{\mathrm{i}} z^{\mathrm{i}} z^{\mathrm{r}} + 2\hat{c}_1 z^{\mathrm{i}}(\epsilon_{\mathrm{e}}^{\mathrm{r}})^2 z^{\mathrm{r}} - 2\hat{c}_1 z^{\mathrm{i}}\epsilon_{\mathrm{e}}^{\mathrm{r}}\epsilon_1^{\mathrm{r}} z^{\mathrm{r}}, \tag{7.4}\\
T_4 &= \hat{c}_1^2(\epsilon_{\mathrm{e}}^{\mathrm{i}})^2 z^{\mathrm{i}}(z^{\mathrm{r}})^2 + \hat{c}_1^2 z^{\mathrm{i}}(\epsilon_{\mathrm{e}}^{\mathrm{i}})^2(z^{\mathrm{r}})^2 \tag{7.5}\\
N &= ((\epsilon_{\mathrm{e}}^{\mathrm{i}})^2 z^{\mathrm{i}} - \epsilon_{\mathrm{e}}^{\mathrm{i}}\epsilon_1^{\mathrm{i}} z^{\mathrm{i}} + z^{\mathrm{i}}(\epsilon_{\mathrm{e}}^{\mathrm{r}})^2 - z^{\mathrm{i}}\epsilon_{\mathrm{e}}^{\mathrm{r}}\epsilon_1^{\mathrm{r}} + \epsilon_1^{\mathrm{i}}\epsilon_{\mathrm{e}}^{\mathrm{r}} z^{\mathrm{r}} - \epsilon_{\mathrm{e}}^{\mathrm{i}}\epsilon_1^{\mathrm{r}} z^{\mathrm{r}})|z|^2. \tag{7.6}
\end{aligned}
$$

An upper bound $c_2^{\mathrm{U}}(c_1)$ on the anisotropy parameter c_2 is

$$c_2^{\mathrm{U}} = (F_1 + F_2 + F_3 + F_4)/G, \qquad (7.7)$$

where

$$
\begin{aligned}
F_1 &= -(\epsilon_{\mathrm{e}}^{\mathrm{i}})^2 z^{\mathrm{i}} + 2\epsilon_{\mathrm{e}}^{\mathrm{i}}\epsilon_2^{\mathrm{i}} z^{\mathrm{i}} - (\epsilon_2^{\mathrm{i}})^2 z^{\mathrm{i}} - c_1^2(\epsilon_2^{\mathrm{i}})^2(z^{\mathrm{i}})^3 - 2c_1\epsilon_2^{\mathrm{i}}(z^{\mathrm{i}})^2\epsilon_{\mathrm{e}}^{\mathrm{r}}, &(7.8)\\
F_2 &= -z^{\mathrm{i}}(\epsilon_{\mathrm{e}}^{\mathrm{r}})^2 + 2c_1\epsilon_{\mathrm{e}}^{\mathrm{i}}(z^{\mathrm{i}})^2\epsilon_2^{\mathrm{r}} + 2z^{\mathrm{i}}\epsilon_{\mathrm{e}}^{\mathrm{r}}\epsilon_2^{\mathrm{r}} - z^{\mathrm{i}}(\epsilon_2^{\mathrm{r}})^2 - c_1^2(z^{\mathrm{i}})^3(\epsilon_2^{\mathrm{r}})^2, &(7.9)\\
F_3 &= 2c_1\epsilon_{\mathrm{e}}^{\mathrm{i}}\epsilon_2^{\mathrm{i}} z^{\mathrm{i}} z^{\mathrm{r}} - 2c_1(\epsilon_2^{\mathrm{i}})^2 z^{\mathrm{i}} z^{\mathrm{r}} + 2c_1 z^{\mathrm{i}}\epsilon_{\mathrm{e}}^{\mathrm{r}}\epsilon_2^{\mathrm{r}} z^{\mathrm{r}} - 2c_1 z^{\mathrm{i}}(\epsilon_2^{\mathrm{r}})^2 z^{\mathrm{r}}, &(7.10)\\
F_4 &= -c_1^2(\epsilon_2^{\mathrm{i}})^2 z^{\mathrm{i}}(z^{\mathrm{r}})^2 - c_1^2 z^{\mathrm{i}}(\epsilon_2^{\mathrm{r}})^2(z^{\mathrm{r}})^2, &(7.11)
\end{aligned}
$$

and

$$G = (\epsilon_{\mathrm{e}}^{\mathrm{i}}\epsilon_2^{\mathrm{i}} z^{\mathrm{i}} - (\epsilon_2^{\mathrm{i}})^2 z^{\mathrm{i}} + z^{\mathrm{i}}\epsilon_{\mathrm{e}}^{\mathrm{r}}\epsilon_2^{\mathrm{r}} - z^{\mathrm{i}}(\epsilon_2^{\mathrm{r}})^2 + \epsilon_2^{\mathrm{i}}\epsilon_{\mathrm{e}}^{\mathrm{r}} z^{\mathrm{i}} - \epsilon_{\mathrm{e}}^{\mathrm{i}}\epsilon_2^{\mathrm{r}} z^{\mathrm{r}})|z|^2.$$

References

[1] G. A. Baker. *Essentials of Padé Approximants.* Academic Press, New York, 1975.

[2] D. J. Bergman. The dielectric constant of a composite material - a problem in classical physics. *Physical Reports*, **43**(9), 377–407, 1978.

[3] E. Cherkaeva. Inverse homogenization for evaluation of effective properties of a mixture. *Inverse Problems*, **17**, 1203–1218, 2001.

[4] E. Cherkaeva and K. M. Golden. Inverse bounds for microstructural parameters of composite media derived from complex permittivity measurements. *Waves in Random Media*, **8**, 437–450, 1998.

[5] E. Cherkaeva and A. C. Tripp. Inverse conductivity for inaccurate measurements. *Inverse Problems*, **12**, 869–883, 1996.

[6] A. R. Day and M. F. Thorpe. The spectral function of composites: the inverse problem. *J. Phys.–Condensed Matter*, **11**, 2551–2568, 1999.

[7] C. Engström. Bounds on the effective tensor and the structural parameters for anisotropic two-phase composite material. *J. Phys. D: Applied Phys.*, **38**, 3695–3702, 2005.

[8] C. Engström. Inverse bounds and bulk properties of complex-valued two-component composites. Technical Report LUTEDX/(TEAT-7141)/1–24/(2005), Lund Institute of Technology, Department of Electroscience, P.O. Box 118, S-221 00 Lund, Sweden, 2005. `http://www.es.lth.se`.

[9] J. I. Gittleman, B. Abeles, P. Zanzucchi, and Y. Arie. Optical properties and selective solar absorption of composite material films. *Thin Solid Films*, **45**, 9–18, 1977.

[10] K. Golden and G. Papanicolaou. Bounds for effective parameters of heterogeneous media by analytic continuation. *Communications in Mathematical Physics*, **90**, 473–491, 1983.

[11] P. B. Johnson and R. W. Christy. Optical constants of the noble metals. *Phys. Rev. B*, **6**(12), 4370–4379, 1972.

[12] R. C. McPhedran, D. R. McKenzie, and G. W. Milton. Extraction of structural information from measured transport properties of composites. *Applied Physics A*, **29**(1), 19–27, 1982.

[13] R. C. McPhedran and G. W. Milton. Inverse transport problems for composite media. *Material Resources Society, Symposium Proceedings*, **195**, 257–277, 1990.

[14] G. W. Milton. Bounds on the transport and optical properties of two-component composite material. *J. Appl. Phys.*, **52**(8), 5294–5304, 1981.

[15] G. W. Milton. *The Theory of Composites*. Cambridge University Press, Cambridge, U.K., 2002.

[16] E. D. Palik. *Handbook of Optical Constants of Solids*. Academic Press, New York, 1985.

[17] S. Torquato. *Random Heterogeneous Materials: Microstructure and Microscopic Properties*. Springer-Verlag, Berlin, 2002.